A MEASUREMENT DATA-BASED INVESTIGATION OF FADING MODELING FOR INDOOR THz WIRELESS SYSTEMS

Evangelos N. Papasotiriou[1], Alexandros-Apostolos A. Boulogeorgos[1], Angeliki Alexiou[1]
[1]Department of digital systems, University of Piraeus research center, 18534, Piraeus, Greece

NOTE: Corresponding author: Evangelos N. Papasotiriou, vangpapasot@unipi.gr

Abstract *– The terahertz (THz) band offers a vast amount of still unallocated bandwidth, which makes it a promising enabler for future sixth generation wireless systems. The high frequencies of the THz band lead to a significantly reduced multipath richness of the propagating THz signals. However, there are still paths that can carry a significant amount of power. As a result, the THz band small-scale fading characterization is of particular interest and the appropriate stochastic distributions that best fit the empirical channels need to be identified. This work investigates the suitability of the* $\alpha-\mu$*, Rice and Nakagami-m distributions to adequately model the small-scale fading statistics of the channel gain measurements of various Line-of-Sight (LoS) and Non-Line-of-Sight (NLoS) indoor THz wireless links. The fitting accuracy of the examined analytical distributions is validated by means of the Kolmogorov-Smirnov test, the Kullback-Leibler divergence, the logarithmic Kolmogorov-Smirnov test and the root-mean-square-error. Also, the ergodic capacity based on the channel gain measurements as well as on the* $\alpha-\mu$*, Rice and Nakagami-m distributions is presented. Based on the fitting accuracy metrics the Rice and* $\alpha-\mu$ *yield the best fit for the LoS and NLoS links, respectively. The Nakagami-m does not fit the empirical distributions for any of the presented links. Furthermore, insights are provided for the ranges of the extracted values of the analytical distributions in LoS and NLoS transmission conditions.*

Keywords – $\alpha-\mu$, experimental results, fitting, Nakagami-m distribution, Rice distribution, small-scale fading, THz wireless communications

1. INTRODUCTION

The terahertz (THz) band spans the vast frequency range of 0.1–10 THz. It offers a contiguous bandwidth of more than 20 gigahertz (GHz) [1, 2], which makes it a promising enabler for the sixth Generation $(6G)$ wireless technologies. From the beginning of the previous decade, both the academics and industry have focused their efforts in developing oudoor and especially indoor THz wireless systems [2–5]. Especially for indoor THz wireless communications, major standardization bodies are in the process of publishing spectrum allocation standards and regulations. More specifically, such published standards are the Institute of Electrical and Electronics Engineers (IEEE) Standard (Std.) $802.15.3$d–2017 [6], International Telecommunication Union (ITU)-T SM. 2353 report 2015 and 2016 [7], European Telecommunications Standards Institute (ETSI) millimeter Wave Transmission (mWT) [8], Federal Communications Commission (FCC): American spectrum regulations [9] and the European Communications Commission (ECC): Europe spectrum relations [10].

The high frequencies of the THz band lead to severe propagation losses for the transmitted signals. Hence, the wireless THz transmissions heavily depend on the Line-of-Sight (LoS) component of the received signal [11–13]. In this direction, the THz channel is often modeled by taking into consideration only the large scale propagation phenomena, which are the deterministic path-loss and shadowing [11, 12, 14–20]. In the THz band the de- terministic path-loss is given as the product of the free space and molecular absorption loss [11]. The molecular absorption loss is modeled with the aid of spectroscopic databases, which contain the various molecular absorption lines needed [3]. However, this is a tedious procedure and several simplified molecular absorption loss models have been developed spanning different ranges of the THz band. Such models are [11], [15] and [16], which were employed in the ranges of 100–450 GHz, 200–450 GHz and 275–400 GHz, respectively. In these models the THz channel was assumed to consist of a single LoS coefficient, which was expressed as the product of the free space and the molecular absorption loss. In [12] and [14], LoS and Non-Line-of-sight (NLoS) channel measurements for indoor wireless links operating at 28 GHz and 140 GHz were performed. This work made use of the measured received signal power of the multipath components in order to model the millimeter wave (mmWave) and THz channels as the deterministic sum (in dB) of an exponential path-loss and a log-normal shadowing distribution. In more detail, in [12] and [14], the exponential path-loss parameter and the variance of shadowing were extracted by employing the received signal powers of the measured links. In [18] and [20], a single path theoretical THz channel model for nano-scale machine communications within vegetation was developed, where the receiver (RX) was assumed to detect signals only from the LoS direction. The channel was assumed to be

composed of two coefficients, namely the path-loss and the log-normal shadowing.

The THz wireless transmissions heavily rely on the existence of the LoS component of the propagating signal. Despite this fact, there are aerosols in the atmospheric medium, as well as objects laid in the propagation environment that can act as scatterers [12, 14] and [21]. This suggests that there are NLoS THz multipath components with significant power capable of being detected by the RX. The presence of multipath components with different received power levels, angles of arrival and delay times means that the received signal power at the RX can have deep and time varying fast fades [22]. According to [22], these phenomena are parts of the stochastic small-scale fading.

Scanning the technical literature, several pieces of work can be identified that conduct theoretical as well as experimental THz channel modeling by taking into account the small-scale fading phenomena [3, 4, 12, 14, 17, 23–30]. In [3], it was observed that, according to THz channel measurements the small-scale fading can be modeled by means of Rice, Nakagami-m and Rayleigh distributions. This remark was employed in [3] and [27], where the more generic α–μ distribution was used to model the small-scale fading and evaluate the performance under different levels of transceivers' antenna misalignment, hardware impairments and various levels of fading severity, for a backhaul THz wireless system. In [30] and [23], a two dimensional geometric channel model for indoor THz communications was developed. The resulting model led to the creation of a parametric multipath Rice fading channel model. In [29], an indoor stochastic THz channel model was presented, where the small-scale fading attenuation factor was expressed as a Rayleigh or Nakagami-m distribution under NLoS conditions and as a Rice or Nakagami-m in LoS. This model was validated by performing experimental measurements in an anechoic chamber.

The authors in [24], exploited the LoS and NLoS links, which were measured in the premises of a shopping mall. The measurements were used to derive a suitable small-scale fading distribution for wireless THz systems operating at 140 GHz. This work concludes that, at least for the used links the distribution that most accurately fits the data is the Weibull in LoS and Nakagami-m in NLoS conditions. The fitting accuracy of the exploited distributions was evaluated in terms of the Kolmogorov-Smirnov (KS) test. In [4], a small-scale fading distribution expressed as the sum of individual Gamma distributions was developed for THz wireless systems operating in the range of 240–300 GHz. The suitability of the proposed distribution was evaluated by fitting it to channel measurements. The used fitting accuracy metrics were the KS, Kullback Leibler (KL) divergence test and the weighted relative mean difference error metric. In [17], a measurement-based THz channel model for LoS and NLoS links operating in the range of 126–156 GHz was proposed. This model relied on the extended Saleh-Valenzuela channel model.

In [25], a theoretical small-scale fading channel model for a holographic multiple-input-multiple-output system operating in the mmWave or the THz band was developed. The small-scale fading was modeled as a zero-mean spatially stationary and correlated Gaussian scalar random field. In [28], the suitability of the α– μ distribution to describe the small-scale fading statistics of indoor LoS and NLoS links operating at 142 GHz was investigated. The fitting accuracy of examined distribution to the channel measurements was evaluated in terms of the KS test. Also, the ergodic capacity was calculated for indicative values of the parameters α and μ. In [26], the fitting accuracy of α– μ, Rice, Rayleigh, log-normal and Nakagami-m distributions to indoor THz channel measurements was investigated. In more detail, the employed indoor LoS and NLoS measurements took place in three different locations and time periods. The fitting accuracy of the analytical distributions was evaluated in terms of the KS and the KL divergence tests. By making use of the metrics it was concluded that, the small-scale fading statistics of all the examined links are best described by means of the α– μ distribution.

In this work the LoS and NLoS THz links of an indoor measurement environment were exploited. The measurements were conducted in May 2021 within an entrance hall of Aalto university in Finland. For each of the presented links multiple channel gain measurements were recorded. These channel gain measurements are employed in order to investigate the suitability of the α–μ, Rice and Nakagami-m distributions to adequately describe the small-scale fading statistics of THz wireless links. To study the small-scale fading characteristics of a link, a preprocessing and an increment of channel realizations method must be first applied to the channel gain measurements. By employing the resulting channel gain measurements realizations of each link, the analytical expressions of the Probability Density Function (PDF) and Cumulative Density Function (CDF) of α– μ, Rice and Nakagami-m are fitted to the corresponding empirical distributions. The parameters of the analytical distributions are obtained by fitting them to the empirical ones of the channel gain for each of the presented links. To achieve this non-linear regression machine learning is used. Furthermore, the Ergodic Capacity (EC) obtained by means of α– μ, Rice and Nakagami-m as well as the EC based on the empirical data of the links are presented. The fitting accuracy metrics and the EC expressions provide useful insights for the purposes of indoor THz small-scale fading statistics. Specifically, from the fitting accuracy metrics it is revealed that in LoS transmission conditions the Rice distribution should be used, whereas in NLoS the α– μ. Finally, the metrics provide insights about the values and ranges of the employed analytical distribution parameters in LoS and NLoS transmission scenarios.

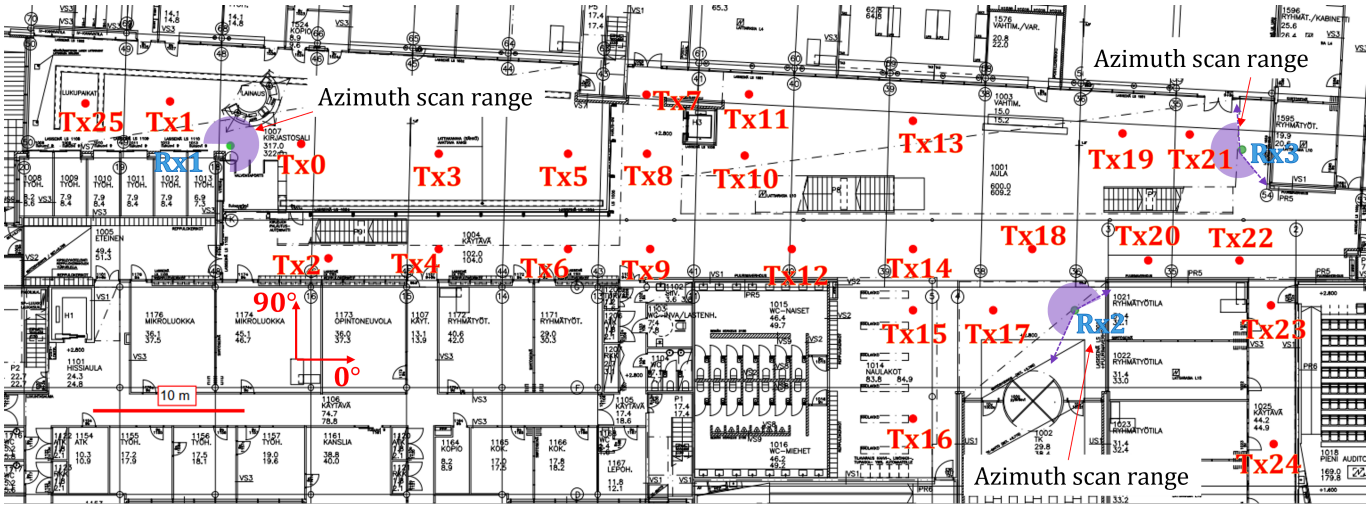

Fig. 1 – Top view of the measurement environment

The remainder of this paper is organized as follows. Section 2 briefly presents the experimental measurements setup. Section 3.1 shows the preprocessing method applied to the channel gain measurements of each link. Section 3.2 presents the method for increasing the channel realizations of a link. Section 3.3 shortly revisits the fundamentals of the $\alpha-\mu$, Rice and Nakagami-m distributions. Section 3.4 briefly presents the employed fitting accuracy metrics. Section 4 presents the EC expressions calculated by employing the $\alpha-\mu$, Rice and Nakagami-m distributions. Section 5 presents for each link the calculated parameters of the employed distributions, the results of the fitting accuracy metrics, the achieved EC by the chan-nel measurements as well as the EC obtained by means of the investigated distributions. Finally, Section 6 provides the closing remarks of this work.

2. EXPERIMENTAL SETUP

The THz channel measurements that are employed in this work were conducted in an indoor environment within the premises of the Aalto University in Finland. Fig. 1 illustrates a top view of the building, where a transmitter (TX) and a RX pair uniquely identify a measured link. All the measurements were performed in an indoor environment, hence a link could be in LoS conditions or if a link was blocked by obstacles or the transceivers were placed in different rooms, it was in NLoS conditions. During the measurement of each link the TX and the RX were static, while there were not any moving people or objects.

The specifications of the THz channel sounding system utilized in this work can be found in [12, 14, 31, 32]. Finally, it should be noted that, the operational frequency was set equal to 142 GHz and the selected bandwidth was set equal to 4 GHz.

3. FADING CHARACTERIZATION

The following sections present the methodology used to obtain the channel gains of the measured paths for each of the links defined by the TXs and RX_2 and RX_3. It should be noted that the links defined by the TXs and RX_1 are not used in this work. The suitability of the $\alpha-\mu$ distribution to describe the small-scale fading channel amplitude of those links was investigated in [31]. Meanwhile, Section 3.1 presents the preprocessing method applied to obtain the channel gain of the measured paths of each link. In Section 3.2, the technique to increase the channel realizations of a link by introducing a random uniform phase to the measured amplitudes will be shown. Then, Section 3.3, briefly revisits the PDF, CDF and the corresponding parameters definitions of the $\alpha-\mu$, Rice and Nakagami-m distributions. Finally, Section 3.4, provides the definitions of the employed fitting accuracy metrics, which namely are the KS, lgKS, KL and RMSE.

3.1 Preprocessing

The channel of a Radio Frequency (RF) wireless link is composed of the product of two coefficients, one deterministic and one stochastic. The deterministic part of the channel encapsulates the large-scale fading effects of the propagation, i.e. the path-loss. In more detail, the large-scale fading describes the time-invariant phenomena of the signal propagation. The stochastic channel coefficient expresses the small-scale fading characteristics of the channel, which are time and frequency dependent. Furthermore, the small-scale fading can lead to deep unpredicted fades to the received signal power. Hence, in order to perform small-scale fading characterization of the channel the deterministic coefficient must be eliminated.

The channel sounding performed in the building shown in Fig. 1, provides Power Angular Delay Profiles (PADPs) for each of the measured TX–RX_2 and TX–RX_3 links. The

PADPs for each link are expressed as a set of propagation paths

$$\text{PADP}\left(\phi,t\right)=\sum_{i=1}^{I}GP_i\delta\left(\phi-\phi_i\right)\delta\left(t-t_i\right), \qquad (1)$$

where ϕ_i, P_i and t_i stand for the azimuth angle at the RX, the propagation delay gain and time of the i–th propagation path, respectively. The parameter G known as the broadside angle, denotes the combined gains of the TX and RX antennas, while I and $\delta\left(\cdot\right)$ are the total number of multipath components of a link and the Dirac delta function, respectively. Then, in order to eliminate the deterministic phenomenon of path-loss, the link path gain measurements are normalized to unity as

$$\zeta_i^2=\frac{P_i}{\overline{p}}, \qquad (2)$$

where

$$\overline{p}=\frac{\sum_{i=1}^{I}P_i}{I}. \qquad (3)$$

3.2 Incrementing link channel realizations

The THz band experiences much higher propagation losses in comparison with the mmWave and Ultra-High-Frequency (UHF) bands [11, 12, 33]. In more detail, the THz free space attenuation losses even at a communication distance of one meter and an operational frequency of 140 GHz can be in the excess of 75 dB [5, 11, 14]. Also, the atmospheric water vapor causes severe attenuation to the propagating THz signal [5, 11]. Furthermore, the wavelength of the transmitted THz electromagnetic wave is much smaller compared to the size of obstacles laid within the propagation path [13]. Hence, the reflection and refraction losses of the THz band are signi-ficantly stronger in comparison with the lower frequency bands [33–36]. This leads in the reduction of the number of dominant rays, since the THz signal power becomes drastically weaker when it is reflected or scattered two or more times [13, 34]. Accordingly, the ability of the THz electromagnetic wave to propagate through blockages is nearly lost due to the severe penetration loss. As a result, the capability of the THz signals to diffract around obstacles is significantly reduced. For example, in [36] 45.6 dB of attenuation were observed at 310 GHz when the transmission was obstructed by a human hand. Based on the aforementioned remarks, it is clear that the THz band yields non-rich multipath environments, when com- pared to lower frequency bands such as the mmWave. De- spite this fact, there are surfaces that can act as scatterers in the THz band [12, 14, 17, 23, 33]. This leads to the existence of reflected NLoS multipath components carrying a significant amount of power capable of being detected by the RX. Nevertheless, the number of measured multi-path components, utilized in our analysis, is still not sufficient to perform small-scale fading statistics analysis for a THz channel. To overcome this limitation, different realizations of the transfer function can be realized by changing the phases of the multipath components [37, 38]. The phases are assumed to be stochastic and given by a uniform distribution in the interval $(0,\ 2\pi)$. Then, the channel coefficient of a Single-Input-Single-Output (SISO) system can be obtained as [31, 37, 38]

$$h=\sum_{i=1}\zeta_i\exp\left(-j2\pi ft_i\right)\exp(j\psi_i), \qquad (4)$$

where $\psi_i\ \sim U\left(0,2\,\pi\right)$ represents the random phase of the i–th multipath component and f stands for the frequency. Moreover, by assuming that the amplitude of the channel coefficients does not change dramatically among the progressing t_i, i.e. the channel can be considered as flat-fading then, $t_i=0$ [37]. Also, the term $U\left(\cdot,\cdot\right)$ is the uniform distribution operator [22].

3.3 Fading distributions

According to *(5)* and *(6)* the α– μ distribution offers mathematical tractability. Also, by setting the parameters α and μ to appropriate values many important distributions of the statistical analysis can be obtained, such as the Nakagami-m, Gamma, Rayleigh, Weibull, exponential and one-sided Gaussian [39, 40]. Moreover, it has been extensively employed in studies considering the small-scale fading statistics of RF wireless channels [3, 38, 40]. The PDF and CDF of α– μ are expressed as [39]

$$f\left(x\right)=\frac{\alpha\mu^{\mu}x^{\alpha\mu-1}exp\left(-\mu x^{\alpha}\right)}{\Gamma\left(\mu\right)}, \qquad (5)$$

$$F\left(x\right)=1-\frac{\Gamma\left(\mu,x^{\alpha}\mu\right)}{\Gamma\left(\mu\right)}, \qquad (6)$$

where μ is obtained as [39]

$$\mu=\frac{\mathbb{E}^2\left(X^{\alpha}\right)}{\mathbb{V}\left(X^{\alpha}\right)} \qquad (7)$$

and X is a random variable (r.v.) following the $\alpha-\mu$ distribution. Additionally, $\Gamma\left(\cdot\right)$ and $\Gamma\left(\cdot,\cdot\right)$ stand for the gamma function and the upper incomplete gamma function, respectively [41, eq. (8.310.1)], [41, eq. (8.350.2)]. $\mathbb{E}\left(\cdot\right)$ and $\mathbb{V}\left(\cdot\right)$ represent the expected value and variance, respectively. The parameters $\alpha>0$ and $\mu>0$ stand for the nonlinearity of the received signal envelope due to the propagation environment and the number of the multipath components of the received signal [39], respectively. The non-integer values of μ could indicate non-zero correlation among the in-phase and quadrature parts of the multipath component, non-zero correlation between different clusters of multipath components, or non-Gaussianity of the in-phase and quadrature components of the fading signal [39].

The Rice and Nakagami-m distributions are widely used in modeling the fading statistics of RF wireless channels

[24, 31, 38]. The PDF and CDF of the Nakagami-m distribution are obtained as [22, eq. (3.38)]

$$f_m(x) = \frac{2exp(-mx^2)\, m^m x^{-1+2m}}{\Gamma(m)}, \quad (8)$$

$$F_m(x) = 1 - \frac{\Gamma(m, mx^2)}{\Gamma(m)}, \quad (9)$$

where the parameter m is the fading parameter. The PDF and CDF of the Rice distribution is expressed as [22, eq. (3.37)]

$$f_R(x) = 2x(K+1)\, exp(-K-(K+1)x^2) \times I_o\left(2x\sqrt{K(K+1)}\right), \quad (10)$$

$$F_R(x) = Q_1\left(\sqrt{2}K, 0\right) - Q_1\left(\sqrt{2}K, \frac{x}{\frac{\sqrt{2}}{2}\sqrt{\frac{1}{K+1}}}\right), \quad (11)$$

where $Q_1(\cdot,\cdot)$ is the fisrt order Marcum-Q function [42]. The parameter K denotes the ratio of power of the LoS signal component to the other NLoS signal components, while $I_o(\cdot)$ is the zero order modified Bessel function of the first kind [43, eq. (9.6.3)].

3.4 Analytical distributions fitting accuracy evaluation metrics

The fitting of the examined analytical distributions to the empirical channel gain distribution of each link is evaluated by means of the KS test, the KL divergence, the lgKS test and the RMSE.

The KS goodness of the fit test is defined as [44, eq. (8.320)]

$$max\left(\left|F_{emp}(x) - F(x)\right|\right) \leq \sqrt{-\frac{1}{2N} ln\left(\frac{A}{2}\right)}, \quad (12)$$

where $F_{emp}(\cdot)$, N and $ln(\cdot)$ stand for the empirical values of the channel gain CDF of the examined link, the number of discrete samples of $F_{emp}(\cdot)$ and the natural logarithm respectively. The parameter $F(\cdot)$ stands for the analytical CDF, while $A = 5\%$ is the selected significance level and $x \in [1, N]$. According to the KS the analytical distribution is said to fit the empirical one when the inequality of *(12)* holds true.

The KL divergence is defined as the distance between the empirical PDF $f_{emp}(\cdot)$ and the analytical PDF $f(\cdot)$ of the examined distribution [45]

$$KL = -\sum_x f_{emp}(x)\, ln\left(\frac{f(x)}{f_{emp}(x)}\right), \quad (13)$$

where $x \in [1,\ N]$. The closer the value of *(13)* to 0 the better is the fit of the analytical to the empirical distribution.

In some cases the fitting of the tail of the analytical distribution to the empirical one is of particular interest. For example, such a scenario is the case of severe fading [46, 47]. The statistical test that can yield an appropriate metric regarding the tail fitting is the modified KS test, which from now on will be referred to as the logarithmic scale KS test (lgKS). The lgKS test is expressed as [47, 48]

$$q = \max_x \left|log_{10}\left(F_{emp}(x)\right) - log_{10}\left(F(x)\right)\right|, \quad (14)$$

where $x \in [1, N]$ and $log_{10}(\cdot)$ stands for the logarithm of base 10. It should be noted, that a value of $q = 1$ expresses that there is a difference of one order of magnitude between the analytical and the empirical CDF.

The RMSE is a common fitting accuracy metric. It is applied in many different fields, where the deviation of a function from another one is needed and it is expressed as

$$\text{RMSE} = \sqrt{\frac{1}{N}\sum_x \left(f_{emp}(x) - f(x)\right)^2}, \quad (15)$$

where $x \in [1,\ N]$. The mean square error expresses the mean distance of the analytical distribution to the empirical one. The closer the value of *(15)* to 0, the better the fit achieved by the analytical distribution. The RMSE is commonly used as a fitting evaluation metric in wireless channel modeling [48, 49]. Also, it should be noted that the RMSE is often presented in dB scale [48]. The RMSE values representation in dB scale is also applied in this work as can be seen in Tables 3 and 4.

4. COMMUNICATION PERFORMANCE ASSESSMENT METRICS

An important aspect in evaluating the performance of a wireless system is the EC. In this direction, the EC must be evaluated, when the wireless channel is assumed to be described by each of the examined analytical distributions. Also, the achieved aforementioned EC must be compared to the one based on the measurements of each link.

In THz wireless communications the channel gain of SISO link is expressed as [3]

$$|h| = |h_d|\,|h_f|, \quad (16)$$

where h_d and h_f stand for the deterministic and stochastic channel gain, respectively. Based on *(16)* the instantaneous SNR is expressed as

$$SNR = \kappa\,|h_f|^2, \quad (17)$$

where

$$\kappa = \frac{P_t G_t G_r\,|h_d|^2}{N_o}. \quad (18)$$

The parameters P_t and N_o stand for the transmitted power spectral density and the noise power spectral density at the RX, respectively. Meanwhile, the parameters G_t and G_r denote the TX and RX antenna gains, respectively.

For a THz wireless system where h_f is expressed by the α–μ distribution, the PDF and CDF of the instantaneous SNR after some algebraic manipulations and by using [44, eq. 5.4] and [44, eq. 5.3] can be obtained as

$$f_{SNR_{\alpha\text{-}\mu}}(x) = \frac{\alpha exp\left(-\mu\left(\frac{x}{\kappa}\right)^{\frac{\alpha}{2}}\right)\left(\mu\left(\frac{x}{\kappa}\right)^{\frac{\alpha}{2}}\right)^{\mu}}{2x\Gamma(m)}, \quad (19)$$

$$F_{SNR_{\alpha\text{-}\mu}}(x) = 1 - \frac{\Gamma\left(\mu, \mu\left(\frac{x}{\kappa}\right)^{\frac{\alpha}{2}}\right)}{\Gamma(\mu)}. \quad (20)$$

The EC by employing *(19)* can be obtained as [42]

$$EC_{\alpha\text{-}\mu} = \int_0^{\infty} log_2(1+x) f_{SNR_{\alpha\text{-}\mu}}(x)\, dx. \quad (21)$$

For a THz wireless system where h_f follows the Nakagami-m distribution, the PDF and CDF of the instantaneous SNR after some algebraic manipulations and by using [44, eq. 5.4] and [44, eq. 5.3] can be obtained as

$$f_{SNR_N}(x) = \frac{exp\left(-\frac{mx}{\kappa}\right) m^m \left(\frac{x}{\kappa}\right)^m}{x\Gamma(m)}, \quad (22)$$

$$F_{SNR_N}(x) = 1 - \frac{\Gamma\left(m, \frac{mx}{\kappa}\right)}{\Gamma(m)} \quad (23)$$

The ergdodic capacity by employing *(19)* can be obtained as

$$EC_N = \int_0^{\infty} log_2(1+x) f_{SNR_N}(x)\, dx. \quad (24)$$

For a THz wireless system where h_f follows the Rice distribution, the PDF and CDF of the instantaneous SNR after some algebraic manipulations and by using [44, eq. 5.4] and [44, eq. 5.3] can be obtained as

$$f_{SNR_R}(x) = 2x(K+1) exp\left(-K-(K+1)x^2\right) \times I_o\left(2x\sqrt{K(K+1)}\right), \quad (25)$$

$$F_{SNR_R}(x) = Q_1\left(\sqrt{2K}, 0\right) - Q_1\left(\sqrt{2K}, \sqrt{\frac{2x(K+1)}{\kappa}}\right). \quad (26)$$

The ergdodic capacity by employing *(19)* can be obtained as

$$EC_R = \int_0^{\infty} log_2(1+x) f_{SNR_R}(x)\, dx. \quad (27)$$

5. NUMERICAL RESULTS

In this section, the fitting accuracy of the α–μ, Rice, and Nakagami-m distributions to the empirical channel gain distributions of the links defined by the TXs and RX_2 and RX_3, is presented. Also, the applicability of the presented framework in the evaluation of the EC of the corresponding wireless links is examined. Furthermore, the range of the calculated distribution parameters provides useful insights regarding the small-scale fading channel modeling of LoS and NLoS THz wireless links. Additionally, the values of the fitting accuracy metrics aid in locating the most suitable distribution to model the small-scale fading of a THz wireless link.

Tables 1 and 2 respectively present the extracted parameters of the examined distributions for the links defined by a TX and RX_2 and RX_3. The TX column in these tables contains the index of the particular TX–RX link. The d column stands for the TX–RX separation distance. The LoS column in these tables indicates whether the considered link is in LoS or NLoS. According to Table 1, the ranges of the examined distribution parameters of the LoS links defined by RX_2 are $\alpha \in [3\text{–}\ 3.3]$, $\mu \in [0.75\text{–}\ 2.11]$, $m \in [1.6\text{–}\ 4.4]$ and $K \in [1.9\text{–}\ 7.5]$. For the NLoS links defined by RX_2 it is observed that the extracted distribution parameters presented in Table 1 are within the ranges $\alpha \in [2.07\text{–}\ 3.17]$, $\mu \in [0.65\text{–}\ 0.95]$, $m \in [1\text{–}\ 1.55]$ and $K \in [0.14\text{–}\ 1.7]$. Meanwhile, from Table 2, the parameters of the LoS links defined by RX_3 are within the ranges $\alpha \in [2.8\text{–}\ 3.12]$, $\mu \in [0.61\text{–}\ 1.2]$, $m \in [1.07\text{–}\ 2.6]$, and $K \in [0.63\text{–}\ 3.87]$. For the NLoS links defined by RX_3 the distribution parameters of Table 2 are within the ranges $\alpha \in [2.04\text{–}\ 5.27]$, $\mu \in [0.35\text{–}\ 1.45]$, $m \in [1.006\text{–}\ 3.09]$, and $K \in [0.18\text{–}\ 4.85]$.

Table 1 – Distribution parameters for RX_2 links

TX	LoS	d (m)	α	μ	m	K (dB)
2	✗	47.22	2.078	0.952	1.009	0.198
3	✗	39.57	2.282	0.863	1.054	0.474
4	✗	38.67	2.067	0.954	1.003	0.149
5	✗	32.08	2.46	0.775	1.057	0.516
6	✗	30.95	2.449	0.785	1.064	0.539
7	✗	28.71	2.25	0.872	1.041	0.419
8	✗	27.13	3.054	0.756	1.476	1.605
9	✗	25.93	2.245	0.886	1.057	0.473
10	✗	20.46	2.136	0.925	1.022	0.301
11	✗	22.56	2.233	0.878	1.038	0.4
12	✗	17.16	3.171	0.748	1.557	1.776
13	✓	15.29	3.217	0.756	1.619	1.904
14	✓	10.64	3.019	1.488	3.094	4.85
15	✓	10.19	3.283	0.989	2.289	3.253
16	✗	10.79	3.069	0.656	1.259	1.123
17	✓	5.02	3.278	1.126	2.642	3.959
18	✓	4.05	2.998	2.11	4.438	7.554
19	✗	10.12	3.073	0.694	1.35	1.332
20	✗	4.65	2.518	0.796	1.13	0.749
21	✗	11.77	2.149	0.927	1.033	0.357
22	✗	9.44	2.173	0.907	1.029	0.344
23	✗	10.72	2.2	0.895	1.035	0.378

Table 2 – Distribution parameters for RX_3 links

TX	LoS	d (m)	α	μ	m	K (dB)
2	✗	58.09	2.195	0.875	1.007	0.247
3	✗	49.02	2.344	0.828	1.052	0.482
4	✗	49.62	2.042	0.978	1.009	0.18
6	✗	41.82	2.293	0.866	1.066	0.52
7	✗	36.2	2.726	0.737	1.18	0.906
8	✗	36.13	2.527	0.773	1.1	0.666
9	✗	36.87	2.161	0.904	1.016	0.285
10	✗	28.93	2.786	0.7	1.154	0.845
11	✗	29.08	2.494	0.799	1.118	0.714
12	✗	28.03	3.127	0.781	1.599	1.858
13	✗	19.19	5.275	0.353	1.434	1.58
14	✗	20.69	2.787	0.66	1.077	0.626
15	✗	21.89	2.351	0.84	1.072	0.548
16	✗	25.48	2.318	0.838	1.047	0.456
17	✗	17.31	3.421	0.664	1.542	1.752
18	✗	13.27	2.727	0.704	1.121	0.747
19	✓	9.07	2.819	0.649	1.076	0.631
20	✗	7.12	3.058	1.457	3.094	4.858
21	✓	3.07	3.123	0.613	1.195	0.971
22	✗	5.55	2.699	0.71	1.112	0.721
23	✓	9.97	3.12	1.205	2.605	3.88
24	✗	17.09	2.926	0.705	1.263	1.128

Tables 3 and 4 evaluate the fitting accuracy of the examined analytical distributions to the empirical PDFs and CDFs of the measured links. These tables encapsulate the PDF fitting accuracy metrics KL and RMSE and the CDF accuracy metric of lgKS. The CDF accuracy KS metric is not shown in Tables 3 and 4, because for all the investigated links, all the examined analytical distributions yield a value below the selected significance level of 5%.

Fig. 2(a) shows the fitting of examined analytical distributions to the empirical channel gain PDFs of the links TX_{14}– RX_2 and TX_{17}– RX_2. The blue circles stand for the empirical channel gain PDFs of the presented links, while the red, orange and green lines stand for the corresponding analytical expressions of α–μ, Rice and Nakagami-m distributions, respectively. The KL and RMSE values of Table 3 show that Rice yields the best fit to the empirical distributions for both of the links. Meanwhile, Nakagami- m does not fit the empirical PDFs of the links. Also, for both TX_{14}– RX_2 and TX_{17}– RX_2, α–μ yields a good fit, except a slight divergence on the left of the empirical distributions.

In Fig. 2(b), the fitting of the examined analytical CDFs to the empirical ones of the links TX_{14}–RX_2 and TX_{17}–RX_2 is presented. The blue circles and stars stand for the empirical CDFs of TX_{14}–RX_2 and TX_{17}–RX_2, respectively. The continuous and dashed red, orange and green lines represent the analytical CDF expressions of α– μ, Rice and Nakagami-m distributions for TX_{14}– RX_2 and TX_{17}– RX_2 respectively. The minimum empirical probability of TX_{17}– RX_2 is F $(x) = 0.0014$, which is obtained for $x = -9.6$ dB. The minimum empirical probability of TX_{14}– RX_2 is F $(x) = 0.0013$, which corresponds to x = –8.86 dB. Also, for any given x, the empirical probability of TX_{14}– RX_2 is lower compared to that of TX_{17}– RX_2. For example, for $x = -7$ dB the empirical probability of TX_{14}–RX_2 and TX_{17}–RX_2 is F $(x) = 0.003$ and F $(x) = 0.005$, respectively. The previous observations indicate that, the channel propagation conditions of TX_{14}–RX_2 are better compared to those of TX_{17}–RX_2. These findings on the empirical CDFs correspond to the parameter values of the analytical distributions of Table 1. The values of μ, m and K of TX_{14}–RX_2 are greater than those of TX_{17}–RX_2. The parameter α of TX_{14}–RX_2 is lower compared to the one of TX_{17}–RX_2. In more detail, the physical meaning of those parameters verify that stronger multipath components are detected by the RX in the case of TX_{14}–RX_2. Furthermore, the lgKS metric shown in Table 3 and the curves of Fig. 2 demonstrate that the Rice distribution in both of the presented links yields an almost perfect fit to the empirical data.

Fig. 2(c) shows the EC of the links TX_{14}–RX_2 and TX_{17}– RX_2 as a function of κ. The circles and stars stand for the EC achieved by employing the empirical distributions of TX_{14}–RX_2 and TX_{17}–RX_2, respectively. The continuous and dashed red, orange and green lines represent the EC obtained by making use of the analytical expressions of α–μ, Rice and Nakagami-m for the TX_{14}– RX_2 and TX_{17}– RX_2 links, respectively. The empirical curves show that for any given value of κ, the EC of TX_{14}– RX_2 is always greater compared to the one TX_{17}–RX_2. This remark is in accordance with the observation made on Fig. 2(b), which states that TX_{14}– RX_2 has better channel conditions com- pared to TX_{17}– RX_2. As an example, for $\kappa = 16$ dB the empirical EC of TX_{14}– RX_2 and TX_{17}– RX_2 is 5.1 (bps/Hz) and 5.06 (bps/Hz), respectively. As Fig. 2(c) illustrates the EC curves obtained by employing the Rice distribution closely follow the empirical ones, whereas the α–μ EC curves slightly diverge. For example, for TX_{14}–RX_2 and $\kappa = 24$ dB the empirical, Rice and α–μ obtained EC is 7.71, 7.72, and 7.73 bps/Hz, respectively. The Nakagami-m EC curves show the greatest divergence from the empirical ones. For both TX_{14}– RX_2 and TX_{17}– RX_2, the EC obtained by means of Nakagami-m can be considered as an upper bound. For example, for TX_{14}– RX_2 and $\kappa = 30$ dB the em- pirical and Nakagami-m EC is 9.69 and 9.78 bps/Hz, respectively. Also, for TX_{17}– RX_2 and $\kappa = 30$ dB the empir- ical and Nakagami-m EC is 9.65 and 9.75 bps/Hz, respectively.

Fig. 3(a) shows the fitting achieved by α–μ, Rice and Nakagami-m distributions to the empirical PDFs of links TX_5– RX_2 and TX_{16}– RX_2. The blue circles and the red, orange and green lines stand for the empirical PDFs, the α–μ, Rice and Nakagami-m analytical PDFs, respectively. The KL and RMSE metrics of Table 3 for the presented links state that the α–μ performs a better fit to the empirical data compared to that achieved by Rice and Nakagami-m. From this figure, it is observed that for both TX_5– RX_2 and TX_{16}– RX_2 Nakagami-m does not fit the empirical curves. The curve of Rice diverges from

Table 3 – Fitting evaluation metrics for RX_2 links.

TX	$KL_{\alpha-\mu}$	KL_R	KL_N	$lgKS_{\alpha-\mu}$	$lgKS_R$	$lgKS_N$	$RMSE_{\alpha-\mu}$ (dB)	$RMSE_R$ (dB)	$RMSE_N$ (dB)
2	0.019	0.019	0.023	0.124	0.138	0.151	−19.94	−19.92	−19.82
3	0.021	0.023	0.083	0.154	0.17	0.254	−20.15	−20.14	−18.84
4	0.017	0.018	0.021	0.13	0.149	0.153	−20.33	−20.3	−20.23
5	0.046	0.076	0.199	0.097	0.166	0.25	−19.27	−18.93	−17.31
6	0.03	0.048	0.159	0.107	0.162	0.258	−19.5	−19.27	−17.52
7	0.015	0.016	0.057	0.134	0.158	0.221	−20.15	−20.18	−19.09
8	0.025	0.019	0.419	0.312	0.124	0.822	−19.19	−19.63	−14.96
9	0.016	0.015	0.066	0.166	0.167	0.255	−20.21	−20.21	−19.16
10	0.016	0.016	0.031	0.152	0.165	0.2	−20.2	−20.23	−19.81
11	0.025	0.026	0.073	0.127	0.151	0.208	−19.41	−19.45	−18.68
12	0.035	0.03	0.539	0.341	0.125	0.94	−18.95	−19.57	−14.6
13	0.048	0.032	0.571	0.431	0.18	1.08	−18.5	−19.13	−14.46
14	0.211	0.031	0.928	0.901	0.149	1.749	−17.58	−18.6	−14.89
15	0.109	0.05	1.013	0.692	0.076	1.663	−18.87	−18.53	−14.3
16	0.017	0.072	0.449	0.192	0.204	0.591	−18.74	−17.99	−14.83
17	0.13	0.049	1.006	0.658	0.089	1.571	−17.61	−17.8	−14.15
18	0.067	0.035	0.45	0.376	0.034	0.983	−17.74	−17.73	−15.11
19	0.016	0.038	0.441	0.228	0.158	0.679	−19.97	−19.58	−15.06
20	0.013	0.019	0.158	0.15	0.144	0.342	−20.14	−20.02	−17.42
21	0.017	0.016	0.035	0.153	0.154	0.206	−19.89	−19.89	−19.5
22	0.016	0.016	0.039	0.129	0.145	0.189	−21.32	−21.34	−20.46
23	0.019	0.02	0.052	0.168	0.185	0.238	−19.76	−19.76	−19.14

Table 4 – Fitting evaluation metrics for RX_3 links.

TX	$KL_{\alpha-\mu}$	KL_R	KL_N	$lgKS_{\alpha-\mu}$	$lgKS_R$	$lgKS_N$	$RMSE_{\alpha-\mu}$ (dB)	$RMSE_R$ (dB)	$RMSE_N$ (dB)
2	0.016	0.018	0.033	0.117	0.175	0.182	−20.04	−19.73	−19.36
3	0.019	0.024	0.087	0.154	0.194	0.272	−20.21	−20.09	−18.63
4	0.021	0.02	0.024	0.186	0.186	0.201	−19.39	−19.39	−19.36
6	0.016	0.016	0.068	0.162	0.166	0.268	−19.79	−19.77	−18.64
7	0.015	0.027	0.233	0.161	0.159	0.429	−19.86	−19.6	−16.34
8	0.015	0.022	0.141	0.114	0.147	0.297	−19.85	−19.71	−17.19
9	0.02	0.022	0.043	0.22	0.262	0.293	−19.9	−19.9	−19.46
10	0.017	0.044	0.267	0.116	0.159	0.39	−19.58	−18.95	−15.92
11	0.016	0.015	0.115	0.148	0.149	0.327	−20.15	−20.16	−17.57
12	0.034	0.031	0.547	0.409	0.143	1.016	−18.88	−19.25	−14.65
13	0.057	0.651	1.509	0.045	0.198	0.832	−16.81	−12.6	−11.05
14	0.057	0.159	0.378	0.048	0.178	0.289	−18.4	−17.27	−15.55
15	0.019	0.021	0.092	0.175	0.189	0.299	−19.22	−19.21	−18.03
16	0.021	0.026	0.09	0.125	0.163	0.234	−19.57	−19.53	−18.3
17	0.021	0.081	0.685	0.304	0.171	0.966	−19.6	−17.96	−14.03
18	0.024	0.066	0.273	0.112	0.176	0.357	−18.92	−18.33	−15.98
19	0.047	0.133	0.351	0.079	0.218	0.326	−18.93	−17.44	−15.56
20	0.142	0.028	0.813	0.786	0.071	1.654	−18.03	−18.51	−14.89
21	0.063	0.216	0.62	0.128	0.215	0.505	−19.03	−17.23	−14.44
22	0.032	0.079	0.285	0.114	0.181	0.349	−19.11	−18.47	−16.03
23	0.144	0.032	0.917	0.815	0.07	1.738	−17.76	−18.25	−14.65
24	0.014	0.025	0.318	0.186	0.155	0.548	−19.7	−19.51	−15.41

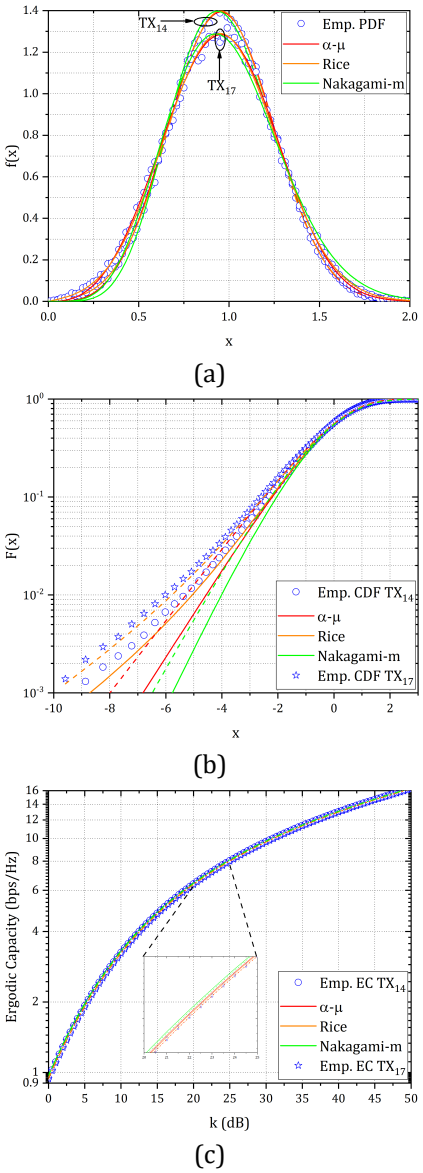

Fig. 2 – Fitting of the analytical to the empirical distributions for the links TX_{14}–RX_2 and TX_{17}–RX_2

the right tail of the empirical PDF of TX_{16}–RX_2. Also, the curve of Rice slightly diverges from the left tail of the empirical PDF of TX_5–RX_2.

In Fig. 3(b), the fitting of the invetigated analytical CDFs to the empirical ones of the links TX_5–RX_2 and TX_{16}–RX_2 is presented. The blue circles and stars stand for the empirical CDFs of TX_{16}–RX_2 and TX_5–RX_2, respectively. The continuous and dashed red, orange and green lines indicate the analytical CDF expressions of TX_{16}–RX_2 and TX_5–RX_2, respectively. The minimum empirical probability for TX_{16}–RX_2 is $F(x) = 0.0026$ for $x = -13.46$ dB. Meanwhile, the minimum empirical probability for TX_5–RX_2 is $F(x) = 0.0031$ for $x = -13.46$ dB. For any given low value of x the empirical probability of TX_{16}–RX_2 is lower compared to that of TX_5–RX_2. As an example, for $x = -9.08$ dB the empirical probability of TX_{16}–RX_2 and TX_5–RX_2 is $F(x) = 0.0105$ and $F(x) = 0.0132$, respectively. The aforementioned results indicate that the channel propagation conditions of TX_{16}–RX_2 are better than those of TX_5–RX_2. The previous observations on the empirical distributions of the links TX_{16}–RX_2 and TX_5–RX_2, have also to be interpreted in terms of the extracted distribution parameters shown in Table 1. In terms of the α–μ, the parameter α of TX_{16}–RX_2 is greater compared to the one of TX_5–RX_2. Meanwhile, the parameter μ of TX_{16}–RX_2 is less than the one of TX_5–RX_2. This remark states that in NLoS conditions, when comparing the channel propagation conditions of two links; the one with the greatest value of α and the lower value of μ has the lowest probability at a greater value of x. In the meantime, the parameters K and m of TX_{16}–RX_2 are greater than those of TX_5–RX_2. This remark states that when comparing two NLoS links the one with the greatest value of K or m has the lowest probability at a greater value of x. This is in accordance with the definition of the Rice and Nakagami-m distribution parameters. Meanwhile, the lgKS values of Table 3 reveal that α–μ performs a better fit to the empirical CDFs compared to Rice and Nakagami-m. Fig. 2(b), illustrates that Nakagami-m for both of the presented links as x decreases significantly deviates from the empirical curves. Moreover, Rice has almost the same fitting performance as α–μ for the link TX_{16}–RX_2, whereas it diverges as x decreases for TX_5–RX_2.

Fig. 3(c) shows the EC of the links TX_5–RX_2 and TX_{16}–RX_2 as a function of κ. The circles and stars stand for the achieved empirical EC of TX_{16}–RX_2 and TX_5–RX_2, respec- tively. The continuous and dashed red, orange and green lines represent the EC expressions obtained by employing the α–μ, Rice and Nakagami-m distributions for the links TX_{16}–RX_2 and TX_5–RX_2, respectively. From the empirical EC curves it is observed that the achieved EC by TX_{16}–RX_2 is greater compared to that of TX_5–RX_2 for any given κ. This observation is in accordance with that of Fig. 3(b), which states that TX_{16}–RX_2 has better channel conditions compared to TX_5–RX_2. For example, for $\kappa = 15$ dB the achieved empirical EC of TX_{16}–RX_2 and TX_5–RX_2 is 4.48 (bps/Hz) and 4.38 (bps/Hz), respectively. Fig. 3(c), illustrates that for both of the examined links the EC curves obtained by means of α–μ closely follow the empirical ones. Meanwhile, for both of the presented links the Rice EC curves slightly diverge from the empirical ones. For example, for TX_{16}–RX_2 and $\kappa = 17$ dB the empirical and α–μ EC is 5.1 bps/Hz, while for $\kappa = 17$ dB Rice yields an EC equal to 5.12 bps/Hz. For both of the examined links, the EC curves obtained by means of the Nakagami-m display an upper bound behavior to the empirical ones. As an example, for the link TX_{16}–RX_2 and $\kappa = 25$ dB the empirical EC and the corresponding Nakagami-m one yield 7.67 and 7.78 bps/Hz, respectively.

Fig. 4(a) illustrates the fitting of the analytical PDFs to the empirical ones of the links TX_{19}–RX_3 and TX_{21}–RX_3.

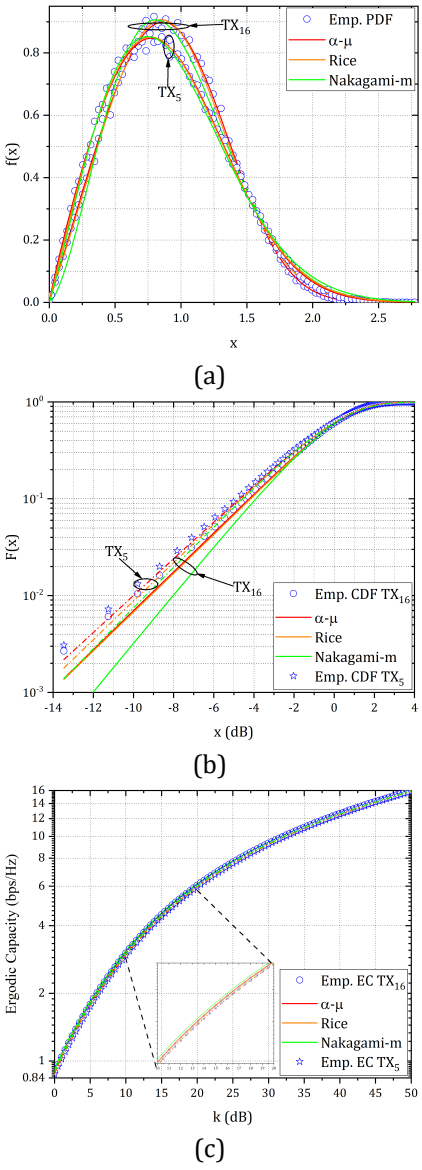

Fig. 3 – Fitting of the analytical to the empirical distributions and their EC performance for the links TX_5–RX_2 and TX_{16}–RX_2.

The blue circles indicate the empirical PDFs of TX_{19}–RX_3 and TX_{21}–RX_3. The red, orange and green continuous and dashed lines stand for the analytical expressions of α–μ, Rice and Nakagami-m for TX_{19}–RX_3 and TX_{21}–RX_3, respectively. Based on the fitting accuracy KL and RMSE metrics of Table 4, α–μ yields the best fit to both of the empirical channel gain distributions. Meanwhile, for both of the presented links, the curve of Rice diverges from the right tail of the empirical PDFs. Furthermore, the curve of Nakagami-m does not fit the empirical distributions of TX_{19}–RX_3 and TX_{21}–RX_3.

In Fig. 4(b), the fitting of the examined analytical distributions to the empirical CDFs of the links TX_{19}–RX_3 and TX_{21}–RX_3 is presented. The blue circles and stars stand for the empirical CDFs of the links TX_{19}–RX_3 and TX_{21}–RX_3, respectively. The continuous and dashed red, orange and green lines represent the analytical expressions of α–μ, Rice and Nakagami-m distributions of TX_{19}– RX_3 and TX_{21}– RX_3, respectively. The minimum empirical probability of TX_{21}– RX_3 and TX_{19}– RX_3 is obtained for $x = -13.47$ dB and is F $(x) = 0.0029$ and F $(x) = 0.0033$, respectively. For any given value of x, especially for the lower ones the empirical probability of TX_{21}– RX_3 is always lower compared to that of TX_{19}– RX_3. As an example, a value of $x = -11.25$ dB yields F $(x) = 0.0077$ and F $(x) = 0.0066$ for TX_{19}– RX_3 and TX_{21}– RX_3, respectively. The previous observations indicate that the channel conditions of TX_{21}– RX_3 are better than those of TX_{19}– RX_3. By considering this, the equivalent connection to the extracted distribution parameters of Table 2 must be performed. In more detail, in terms of the α– μ distribution it is noted that the parameter α of TX_{21}– RX_3 is greater than the one of TX_{19}– RX_3. The parameter μ of TX_{21}– RX_3 is lower than the one of TX_{19}– RX_3. The parameters K and m of TX_{21}– RX_3 are greater compared to those of TX_{19}– RX_3. This is in accordance with the definitions of the Rice and Nakagami-m distribution parameters. In more detail, the greater the value of K or m, the stronger the multipath components of the channel. Furthermore, the lgKS metric of Table 4 and Fig. 4(b), show that as x is reduced for both TX_{19}– RX_3 and TX_{21}– RX_3, α– μ achieves the best fit to the empirical CDFs. Meanwhile, the analytical expressions of Rice and Nakagami-m diverge from the empirical curves of TX_{19}– RX_3 and TX_{21}– RX_3. The Nakagami-m curves perform the worst fit to the empirical distributions of both links.

Fig. 4(c) illustrates the EC of the links TX_{19}– RX_3 and TX_{21}– RX_3 as a function of κ. The circles and stars stand for the achieved EC by the data of TX_{19}– RX_3 and TX_{21}– RX_3, respectively. The continuous and dashed red, orange and green lines represent the EC expressions obtained by means of the α– μ, Rice and Nakagami-m distributions for TX_{19}– RX_3 and TX_{21}– RX_3, respectively. The empirical EC curves state that the EC achieved by TX_{19}– RX_3 link is greater compared to that of TX_{21}– RX_3 for every value of κ. This observation is in accordance with that of fig. 4(b), which states that TX_{19}– RX_3 has better channel conditions compared to TX_{21}– RX_3. As an example, for $\kappa = 30$ dB the empirical EC of TX_{19}– RX_3 and TX_{21}– RX_3 is 9.36 bps/Hz and 9.18 bps/Hz, respectively. As Fig. 4(c), illustrates for both of the examined links, the EC curves obtained by means of α– μ and Rice closely follow the empirical curves. For example, for TX_{19}– RX_3 and $\kappa = 20$ dB the empirical and α– μ EC is 6.08 bps/Hz, while for $\kappa = 20$ dB Rice yields an EC equal to 6.1 bps/Hz. Meanwhile, the Nakagami-m EC curves for both of the links do not diverge significantly from the empirical ones. However, they display an upper bound behavior to the empirical ones.

Fig. 5(a) presents the fitting accomplished by α–μ, Rice and Nakagami-m analytical PDFs to the empirical ones of the links TX_{12}–RX_3 and TX_{20}–RX_3. The blue circles stand for the empirical PDFs of TX_{12}–RX_3 and TX_{20}–RX_3. The red, orange and green lines represent

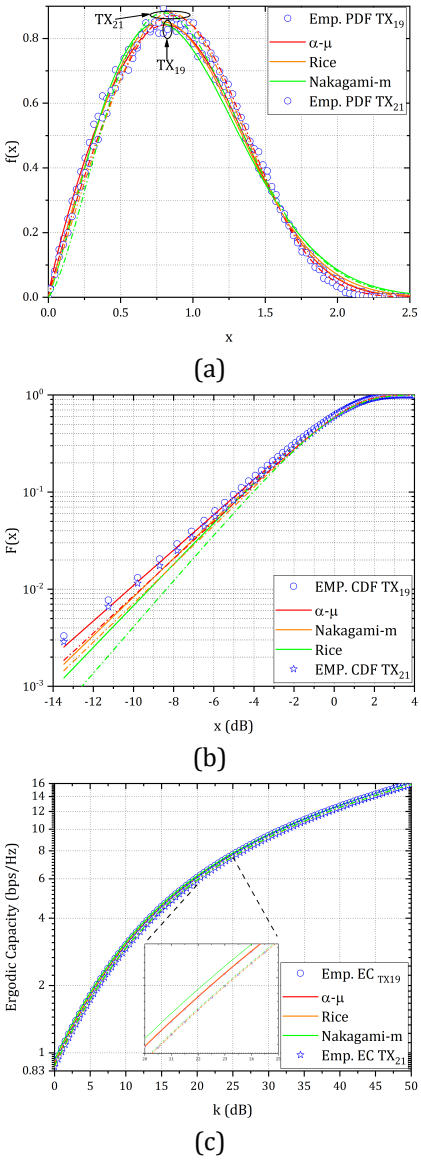

Fig. 4 – Fitting of the analytical to the empirical distributions for the links TX_{19}–RX_3 and TX_{21}–RX_3.

the analytical PDFs of $\alpha-\mu$, Rice and Nakagami-m, respectively. The KL and RMSE metrics of Table 4 reveal that the Rice distribution accomplishes a good fit to the empirical distributions. Meanwhile, on both TX_{12}– RX_3 and TX_{20}– RX_3, $\alpha-\mu$ diverges from the left tail of the empirical distribution, whereas Nakagami-m does not fit the empirical PDFs of the links at all.

In Fig. 5(b), the fitting achieved by the analytical CDFs to the empirical ones of the links TX_{12}–RX_3 and TX_{20}–RX_3 is illustrated. The blue circles stand for the empirical CDFs of TX_{12}–RX_3 and TX_{20}–RX_3. The red, orange and green lines represent the analytically obtained CDFs of $\alpha-\mu$, Rice and Nakagami-m, respectively. The minimum empirical probability for TX_{12}– RX_3 is $F(x) = 0.0015$ for $x = -13.47$ dB. For TX_{20}– RX_3 the minimum empirical probability is $F(x) = 0.0011$ for $x = -8.86$ dB. Further- more, for a given low value of x the empirical probability of TX_{20}– RX_3 is significantly to lower compared that of TX_{12}– RX_3. As an example, a value of $x = -6$ dB yields $F(x) = 0.0345$ and $F(x) = 0.0056$ for TX_{12}– RX_3 and TX_{20}– RX_3, respectively. The aforementioned observations indicate that the channel conditions of TX_{20}– RX_3 are better compared to those of TX_{13}– RX_3. This interpretation of the empirical distributions additionally corresponds to the extracted parameters of the examined analytical distributions, which can be found in Table 2. In more detail, the parameters μ, m and K of TX_{20}– RX_3 are significantly greater compared to those of TX_{12}– RX_3. By taking into account the definition of those parameters, this can be interpreted as the TX_{20}– RX_3 having significantly stronger multipath components detected by the RX, when compared to TX_{20}– RX_3. Furthermore, by observing the curves of the analytical CDFs of this figure and based on the lgKS metric of Table 4, the Rice distribution achieves almost a perfect fit to the empirical data, even as x decreases.

Fig. 5(c) illustrates the EC of the links TX_{12}– RX_3 and TX_{20}– RX_3 as a function of κ. The circles and stars stand for the achieved EC by the data of TX_{12}– RX_3 and TX_{20}– RX_3, respectively. The continuous and dashed red, orange and green lines represent the EC expressions obtained by means of $\alpha-\mu$, Rice and Nakagami-m for TX_{12}– RX_3 and TX_{20}– RX_3, respectively. The empirical EC curves state that the EC achieved by TX_{20}– RX_3 is greater compared to that of TX_{12}– RX_3 for every value of κ. This observation is in accordance with that of Fig. 5(b), which states that TX_{20}– RX_3 has better channel conditions than TX_{12}– RX_3. As an example for $\kappa = 25$ dB the empirical EC of TX_{20}– RX_3 and TX_{20}– RX_3 is 8.05 bps/Hz and 7.78 bps/Hz, respectively. As Fig. 5(c), illustrates for both of the examined links, the EC curves obtained by means of $\alpha-\mu$ and Rice distributions closely follow the empirical ones. For example, for TX_{20}– RX_3 and $\kappa = 30$ dB the empirical and Rice EC is 9.7 bps/Hz, while for $\kappa = 30$ dB $\alpha-\mu$ yields an EC equal to 9.72 bps/Hz. Meanwhile, the EC curves obtained by means of Nakagami-m for both TX_{12}– RX_3 and TX_{20}– RX_3 do not diverge significantly from the empirical ones. However, it is observed that for both of the examined links the EC curves of Nakagami-m display an upper bound behavior to the empirical ones.

Tables 1 and 2, in combination with the observations made on the LoS links presented in figures 2(a)(b) and 4(a)(b) provide insights about the values of the examined distribution parameters. More specifically, when comparing the channel conditions of two LoS links, the one with the better channel conditions, yields greater values for the parameters μ, m and K, while the parameter α obtains a lower value.

By taking into account Tables 1 and 2 combined with the observations made on the NLoS links presented in figures 3(a)(b) and 5(a)(b), insights can be provided regarding the parameter values of the examined distributions. In more detail, when comparing two NLoS links, the one

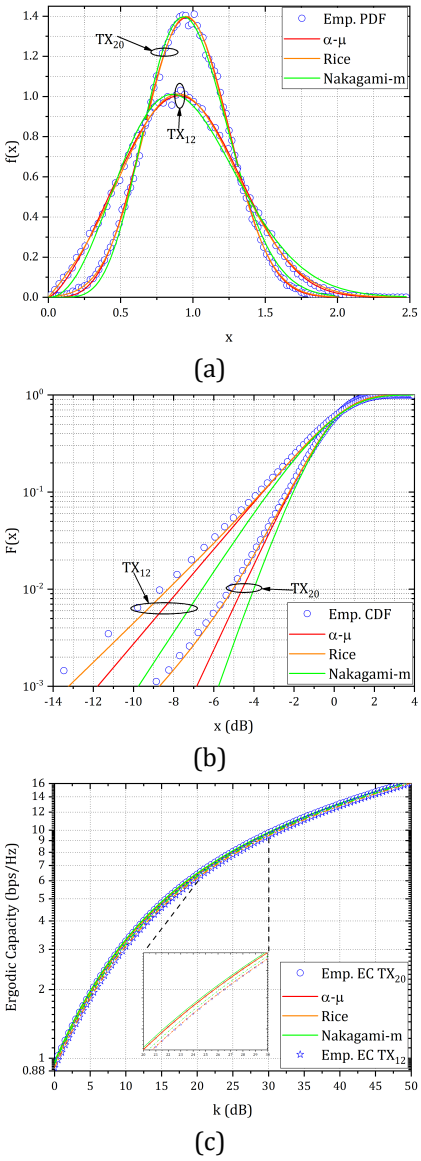

Fig. 5 – Fitting of the analytical to the empirical distributions for the links TX_{12}–RX_3 and TX_{20}–RX_3

with the better channel conditions yields greater values for the parameters α , m and K and a lower value for the parameter μ.

The observations made on the figures 2(a)(b)–5(a)(b) and the fitting accuracy metrics presented in Tables 3 and 4, provide useful insights about the suitability of the examined distributions in terms of small-scale fading statistics of the THz wireless channels. For the LoS transmissions it is deducted that the Rice distribution describes more accurately the fading statistics of the measured channels. However, there are cases where the fitting metrics suggest that the α–μ should be employed instead. Despite this fact, in such scenarios, by observing the metrics of Tables 3 and 4, the difference between the corresponding ones of α–μ and Rice are minor. Furthermore, for the NLoS transmissions it is observed that, the α–μ distribution yields the most accurate fit to the measured channel gains of the investigated links. Meanwhile, there are cases where according to the fitting accuracy metrics the Rice distribution achieves the most accurate fit to the empirical distributions. Despite this fact, in such scenarios the fitting accuracy metrics of Tables 3 and 4 suggest that the difference between the corresponding ones of α–μ and Rice is insignificant. Meanwhile, for all of the presented links according to the KL, RMSE and lgKS metrics it is concluded that the Nakagami-m does not fit the empirical channel gain measurements.

The observations made on the EC performance results presented in figures 2(c)– 5(c) are in accordance with the fitting evaluation of the examined analytical distributions. In more detail, the analytical expression that performs the best fit, also yields the most accurate EC expression, which is almost exact to the empirical one. Furthermore, the EC expressions obtained by means of α–μ, Rice and Nakagami-m yield values quite similar to the empirical ones for every value of κ. However, it is observed that the EC expression of Nakagami-m has the greatest divergence from the empirical values and can be stated that it presents an upper bound behavior to the EC results. Meanwhile, an increase of κ improves the achieved EC. This corresponds to an improvement of the deterministic channel gain, which mitigates the impact of the small-scale fluctuations in the total channel gain of a THz wireless link.

6. CONCLUSION

In this work, the suitability of α–μ, Rice and Nakagami-m distributions was investigated in order to describe the small-scale fading statistics of indoor THz wireless channels. Also, the empirical EC of the measured links was presented and compared to the one achieved by means of the employed analytical distributions. Moreover, useful observations about the ranges and the values of the extracted distributions parameters were made for the LoS and NLoS indoor THz wireless transmission scenarios. The fitting accuracy of the examined distributions was performed by means of the KS, KL, lgKS and RMSE metrics. These metrics revealed that, in LoS transmission conditions the Rice distribution should be employed to model the small-scale fading statistics of the THz channel, whereas in NLoS scenarios α–μ is the most accurate. The fitting accuracy metrics revealed that the Nakagami-m cannot be employed to describe the small-scale fading statistics of the investigated links. Meanwhile, the comparison of two LoS links showed that the one with the better channel conditions has greater values for the parameters μ, m and K and a lower value of α. The comparison of two NLoS links showed that, the one with the better channel conditions yields greater values for the parameters α , m and K and a lower value for μ. By comparing two LoS or NLoS links in terms of the achieved empirical EC it is revealed that, the one having better channel conditions achieves higher EC. Meanwhile, the analytical distribution that leads to the most accurate fit to the empirical

channel gain PDFs and CDFs yields also EC values closer to the empirical ones.

ACKNOWLEDGEMENT

This work has received funding from the European Commission Horizon 2020 research and innovation programme ARIADNE under grant agreement No. 871464.

The indoor propagation channel data used in this work were provided by Aalto University, Finland.

REFERENCES

[1] A.-A. A. Boulogeorgos, A. Alexiou, T. Merkle, C. Schubert, R. Elschner, A. Katsiotis, P. Stavrianos, D. Kritharidis, P. K. Chartsias, J. Kokkoniemi, M. Juntti, J. Lehtomäki, A. Teixeirá, and F. Rodrigues. "Terahertz Technologies to Deliver Optical Network Quality of Experience in Wireless Systems Beyond 5G". In: *IEEE Commun. Mag.* 56.6 (June 2018), pp. 144–151. ISSN:0163-6804.

[2] S Amakawa, Z Aslam, J Buckwater, S Caputo, A Chaoub, Y Chen, Y Corre, M Fujishima, Y Ganghua, S Gao, et al. "White Paper on RF Enabling 6G–Opportunities and Challenges from Technology to Spectrum". In: *Ghent University* (Apr. 2021).

[3] A.-A. A. Boulogeorgos, E. N. Papasotiriou, and A. Alexiou. "Analytical Performance Assessment of THz Wireless Systems". In: *IEEE Access* 7 (Jan. 2019), pp. 11436–11453. ISSN: 2169-3536. DOI: 10.1109/ACCESS.2019.2892198.

[4] K rşat Tekbıyık, Ali Rıza Ekti, G neş Karabulut Kurt, Ali G rçin, and Serhan Yarkan. "Modeling and Analysis of Short Distance Sub-Terahertz Communication Channel via Mixture of Gamma Distribution". In: *IEEE Trans. on Veh. Techn.* 70.4 (Apr. 2021), pp. 2945–2954. DOI: 10.1109/TVT.2021.3063209.

[5] Ian F. Akyildiz and Josep Miquel Jornet. "Electromagnetic wireless nanosensor networks". In: *Nano Commun. Netw.* 1.1 (Mar. 2010), pp. 3–19. ISSN: 1878-7789. DOI:https://doi.org/10.1016/j.nancom.2010.04.001.

[6] "IEEE Standard for High Data Rate Wireless Multi-Media Networks–Amendment 2: 100 Gb/s Wireless Switched Point-to-Point Physical Layer". In: *IEEE Std 802.15.3d-2017 (Amendment to IEEE Std 802.15.3-2016 as amended by IEEE Std 802.15.3e-2017)* (2017), pp. 1–55. DOI:10.1109/IEEESTD.2017.8066476.

[7] "The challenges and opportunities for spectrum management resulting from the transition to digital terrestrial television in the UHF bands". In: *Series SM, Report ITU-R SM.2353-0* (2015).

[8] "ETSI GR mWT 022 V1.1.1 (2021-04): Analysis of Spectrum, License Schemes and Network Scenarios in the RF bands above 174,8 GHz". In: *ETSI* (2021).

[9] "Federal Communications Commission". In: *FCC 19-19* (Mar. 2019).

[10] "European Communications Commition (ECC) Recommendation of 31 January 2014 on radio fre- quency channel arrangements for fixed service sys- tems operating in the band 92-95 GHz." In: *ECC* (2018).

[11] J. Kokkoniemi, L. Janne, and J. Markku. "A line-of-sight channel model for the 100–450 gigahertz frequency band". In: *EURASIP J. on Wir. Commun. and Net.* 88 (Apr. 2021).

[12] S. L. H. Nguyen, J. Järveläinen, A. Karttunen, K. Haneda, and J. Putkonen. "Comparing radio propagation channels between 28 and 140 GHz bands in a shopping mall". In: *12th Eur. Conf. on Ant. and Prop. (EuCAP 2018)*. Apr. 2018, pp. 1–5. DOI: 10.1049/cp.2018.0874.

[13] G. Stratidakis, E. N. Papasotiriou, H. Konstantinis, A.-A. A. Boulogeorgos, and A. Alexiou. "Relay-Based Blockage and Antenna Misalignment Mitigation in THz Wireless Communications". In: *2nd 6G Wir. Sum. (6G SUMMIT)*. Mar. 2020, pp. 1–4.

[14] Sinh L. H. Nguyen, Katsuyuki Haneda, Jan Järveläinen, Aki Karttunen, and Jyri Putkonen. "Large-Scale Parameters of Spatio-Temporal Short-Range Indoor Backhaul Channels at 140 GHz". In: *2021 IEEE 93rd Veh. Techn. Conf. (VTC 2021-Spring)*. Apr. 2021, pp. 1–6. DOI: 10.1109/VTC2021-Spring51267.2021.9448958.

[15] J. Kokkoniemi, J. Lehtomäki, and M. Juntti. "Simple Molecular Absorption Loss Model for 200–450 Gigahertz Frequency Band". In: *2019 Eur. Conf. on Net. and Commun. (EuCNC)*. June 2019, pp. 219–223. DOI:10.1109/EuCNC.2019.8801950.

[16] J. Kokkoniemi, J. Lehtomäki, and M. Juntti. "Simplified molecular absorption loss model for 275-400 gigahertz frequency band". In: *12th Eur. Conf. on Antennas and Propagation (EuCAP)*. London, UK, Apr. 2018.

[17] L. Pometcu and R. D'Errico. "An Indoor Channel Model for High Data-Rate Communications in D-Band". In: *IEEE Access* 8 (Dec. 2020), pp. 9420–9433. DOI:10.1109/ACCESS.2019.2960614.

[18] A. Afsharinejad, A. Davy, B. Jennings, S. Rasmann, and C. Brennan. "A Path-Loss Model Incorporating Shadowing for THz Band Propagation in Vegetation". In: *IEEE Global Communications Conference (GLOBECOM)*. San Diego, CA, USA, Dec. 2015, pp. 1–6. DOI:10.1109/GLOCOM.2015.7417038.

[19] Pavel Boronin, Vitaly Petrov, Dmitri Moltchanov, Yevgeni Koucheryavy, and Josep Miquel Jornet. "Capacity and throughput analysis of nanoscale machine communication through transparency windows in the terahertz band". In: *Nano Commun. Networks* 5.3 (Sept. 2014), pp. 72–82.

[20] A. Afsharinejad, A. Davy, B. Jennings, and C. Brennan. "An initial path-loss model within vegetation in the THz band". In: *9th European Conference on Antennas and Propagation (EuCAP)*. Lisbon, Portugal, May 2015, pp. 1–5.

[21] J. Kokkoniemi, J. Lehtomäki, and M. Juntti. "Frequency domain scattering loss in THz band". In: *Global Symposium on Millimeter-Waves (GSMM)*. Montreal, Canada, May 2015, pp. 1–3. DOI: 10.1109/GSMM.2015.7175457.

[22] Andrea Goldsmith. *Wireless communications*. Cambridge university press, 2005.

[23] S. Kim and A. Zajić. "Statistical Modeling and Simulation of Short-Range Device-to-Device Communication Channels at Sub-THz Frequencies". In: *IEEE Trans. Wireless Commun.* 15.9 (Sept. 2016), pp. 6423–6433. ISSN: 1536-1276. DOI: 10.1109/TWC.2016.2585103.

[24] Dimitrios Selimis, Konstantinos Ntontin, Fotis Lazarakis, and Katsuyuki Haneda. "Initial Investigation of D-band Small-Scale Fading Statistics". In: *15th Eur. Conf. on Ant. and Prop. (EuCAP)*. Mar. 2021, pp. 1–5. DOI: 10.23919/EuCAP51087.2021.9411286.

[25] Andrea Pizzo, Thomas L. Marzetta, and Luca Sanguinetti. "Spatially-Stationary Model for Holographic MIMO Small-Scale Fading". In: *IEEE J. on Sel. Ar. in Commun.* 38.9 (Sept. 2020), pp. 1964–1979. DOI: 10.1109/JSAC.2020.3000877.

[26] Evangelos N Papasotiriou, Alexandros-Apostolos A Boulogeorgos, Katsuyuki Haneda, Mar Francis de Guzman, and Angeliki Alexiou. "An experimentally validated fading model for THz wireless systems". In: *Sc. Rep.* 11.1 (Sept. 2021), pp. 1–14.

[27] A.-A. A. Boulogeorgos, E. N. Papasotiriou, and A. Alexiou. "Analytical Performance Evaluation of THz Wireless Fiber Extenders". In: *IEEE 30th An. Int. Symp. on Per., Indoor and Mob. Radio Commun. (PIMRC)*. Istanbul, Turkey, Sept. 2019, pp. 1–6.

[28] Evangelos N. Papasotiriou, Alexandros-Apostolos A. Boulogeorgos, Mar Francis De Guzman, Katsuyuki Haneda, and Angeliki Alexiou. "A New Look to THz Wireless Links: Fading Modeling and Capacity Assessment". In: *Per. Ind. and Mob. Commun. (PIMRC)*. IEEE, 2021.

[29] A. R. Ekti, A. Boyaci, A. Alparslan, İ. Unal, S. Yarkan, A. Görçin, H. Arslan, and M. Uysal. "Statistical modeling of propagation channels for Terahertz band". In: *IEEE Conf. on Standards for Commun. and Networking (CSCN)*. Helsinki, Finland, Sept. 2017, pp. 275–280. DOI: 10.1109/CSCN.2017.8088634.

[30] S. Kim and A. Zaji . "Statistical modeling of THz scatter channels". In: *9th Eur. Conf. on Antennas and Propagation (EuCAP)*. Lisbon, Portugal, May 2015, pp. 1–5.

[31] Evangelos N. Papasotiriou, Alexandros-Apostolos A. Boulogeorgos, and Angeliki Alexiou. "Fading-Modeling in Indoor THz Wireless Systems". In: *Int. Balkan Conf. on Commun. and Netw. (BalkanCom)*. Sept. 2021, pp. 161–165. DOI: 10.1109/BalkanCom53780.2021.9593181.

[32] Katsuyuki Haneda, Mar Francis De Guzman, Marco Di Renzo, Xuewen Qian, Fadil H. Danufane, Halid Hrasnica, Dimitrios Selimis, Fotis Lazarakis, Antonis Alexandridis, Juhana Lankinen, Tachporn Sanguanpuak, Jukka Lämsä, Joonas Kokkoniemi, Juha Pyhtilä, Pekka Sangi, Santiago Pérez-Peñ a, Domingo Pimienta-del-Valle, Pedro Garcia-del-Pino, José Manuel Riera, Evangelos Papasotiriou, Alexandros-Apostolos A. Boulogeorgos, and Angeliki Alexiou. "D1.2 Channel and Propagation Models". In: *ICT-ARIADNE.EU* (Oct. 2021). DOI: 10.5281/ZENODO.5704666.

[33] Yongzhi Wu, Joonas Kokkoniemi, Chong Han, and Markku Juntti. "Interference and Coverage Analysis for Terahertz Networks With Indoor Block- age Effects and Line-of-Sight Access Point Associ- ation". In: *IEEE Trans. on Wir. Commun.* 20.3 (Nov. 2021), pp. 1472–1486. DOI: 10.1109/TWC.2020.3033825.

[34] Chong Han, A. Ozan Bicen, and Ian F. Akyildiz. "Multi–Ray Channel Modeling and Wideband Characterization for Wireless Communications in the Terahertz Band". In: *IEEE Trans. on Wir. Commun.* 14.5 (May 2015), pp. 2402–2412. DOI: 10.1109/TWC.2014.2386335.

[35] Joonas Kokkoniemi, Janne Lehtomäki, and Markku Juntti. "Stochastic Geometry Analysis for Mean Interference Power and Outage Probability in THz Networks". In: *IEEE Trans. on Wir. Commun.* 16.5 (May 2017), pp. 3017–3028. DOI: 10.1109/TWC.2017.2673844.

[36] Nabil Khalid, Naveed A. Abbasi, and Ozgur B. Akan. "Statistical characterization and analysis of low-THz communication channel for 5G Internet of Things". In: *Nano Commun. Netw.* 22 (Dec. 2019), p. 100258. ISSN: 1878-7789. DOI: https://doi.org/10.1016/j.nancom.2019.100258. URL: https://www.sciencedirect.com/science/article/pii/S1878778918300802.

[37] A. F. Molisch, M. Steinbauer, M. Toeltsch, E. Bonek, and R. S. Thoma. "Capacity of MIMO systems based on measured wireless channels". In: *IEEE Journal on Selected Areas in Communications* 20.3 (Apr. 2002), pp. 561–569. DOI:10.1109/49.995515.

[38] Evangelos N Papasotiriou, Alexandros-Apostolos A Boulogeorgos, Katsuyuki Haneda, Mar Francis de Guzman, and Angeliki Alexiou. "An experimentally validated fading model for THz wireless systems". In: *Sc. Rep.* 11.1 (Sept. 2021), pp. 1–14.

[39] M. D. Yacoub. "The α-μ Distribution: A Physical Fading Model for the Stacy Distribution". In: *IEEE Trans. Veh. Technol.* 56.1 (Jan. 2007), pp. 27–34. ISSN: 0018-9545. DOI: 10.1109/TVT.2006.883753.

[40] Elvio J. Leonardo and Michel D. Yacoub. "The Product of Two α- μ Variates and the Composite α- μ Multipath–Shadowing Model". In: *IEEE Trans. on Veh. Techn.* 64.6 (June 2015), pp. 2720–2725. DOI: 10.1109/TVT.2014.2342611.

[41] I. S. Gradshteyn and I. M. Ryzhik. *Table of Integrals, Series, and Products*. Ed. by Alan Jefrey and Daniel Zwilliger. Academic Press, 2007.

[42] Marvin K Simon and Mohamed-Slim Alouini. *Digital communication over fading channels*. Vol. 95. John Wiley & Sons, 2005.

[43] M. Abramowitz and I. A. Stegun. *Handbook of Mathematical Functions with Formulas, Graphs, and Mathematical Tables*. 9th. New York: Dover Publications, 1972.

[44] A. Papoulis and S.U. Pillai. *Probability, Random Variables, and Stochastic Processes*. McGraw-Hill series in electrical engineering: Commun. and signal processing. Tata McGraw-Hill, 2002. ISBN: 9780070486584.

[45] David J. C. MacKay. *Information Theory, Inference, and Learning Algorithms*. Cambridge University Press, 2003.

[46] Francisco J Cañete, Jesús López-Fernández, Celia García-Corrales, Antonio Sánchez, Encarnació n Robles, Francisco J Rodrigo, and José F Paris. "Measurement and modeling of narrowband channels for ultrasonic underwater communications". In: *Sensors* 16.2 (Feb. 2016), p. 256.

[47] Juan M. Romero-Jerez, F. Javier Lopez-Martinez, José F. Paris, and Andrea J. Goldsmith. "The Fluctuating Two-Ray Fading Model: Statistical Characterization and Performance Analysis". In: *IEEE Trans. on Wir. Commun.* 16.7 (July 2017), pp. 4420–4432. DOI:10.1109/TWC.2017.2698445.

[48] Tiago Reis Rufino Marins, André Antônio dos Anjos, Vicent Miquel Rodrigo Peñarrocha, Lorenzo Rubio, Juan Reig, Rausley Adriano Amaral de Souza, and Michel Daoud Yacoub. "Fading Evaluation in the mm-Wave Band". In: *IEEE Transactions on Communications* 67.12 (Dec. 2019), pp. 8725–8738. DOI:10.1109/TCOMM.2019.2941493.

[49] J.-M. Molina-Garcia-Pardo, M. Lienard, A. Nasr, and P. Degauque. "Wideband analysis of large scale and small scale fading in tunnels". In: *2008 8th International Conference on ITS Telecommunications*. Oct. 2008, pp. 270–273. DOI: 10.1109/ITST.2008.4740269.

AUTHORS

Evangelos N. Papasotiriou was born in Athens, Greece, in 1992. He received a bachelor's degree in computer science from the Department of Computer Science and Biomedical Informatics, University of Thessaly, in 2016, and a master's degree in digital communications and networks from the Department of Digital Systems, University of Piraeus, in 2018. He is currently pursuing a Ph.D. degree in wireless communications. In 2017, he joined the Department of Digital Systems, University of Piraeus, where he conducts research in the area of wireless communications.

Alexandros-Apostolos A. Boulogeorgos (Senior Member, IEEE) was born in Trikala, Greece, in 1988. He received a degree in electrical and computer engineering and Ph.D. degree in wireless communications from the Aristotle University of Thessaloniki (AUTh) in 2012 and 2016, respectively. In 2017, he joined the Department of Digital Systems, University of Piraeus, where he conducts research in the area of wireless communications. From october 2012 to September 2016, he was a teaching assistant with the Department of ECE, AUTh, and from February 2017, he serves as an adjunct professor with the Department of ECE, University of Western Macedonia, and as a visiting lecturer with the Department of Computer Science and Biomedical

Informatics, University of Thessaly. He has authored and co-authored more than 80 technical papers, which were published in scienti ic journals and presented at prestigious international conferences. From october 2012 to September 2016, he was a teaching assistant with the Department of ECE, AUTh, and from February 2017, he serves as an adjunct professor with the Department of ECE, University of Western Macedonia, and as a visiting lecturer with the Department of Computer Science and Biomedical Informatics, University of Thessaly. He has authored and co-authored more than 80 technical papers, which were published in scienti ic journals and presented at prestigious international conferences. Furthermore, he has submitted two (one national and one European) patents. His current research interests span in the area of wireless communications and networks with emphasis on high frequency communications, optical wireless communications, and signal processing and communi- cations for biomedical applications. Dr. Boulogeorgos was awarded the Distinction Scholarship Award from the Research Committee of AUTh in 2014, and was recognized as an Exemplary Reviewer for IEEE COMMUNICATION LETTERS in 2016 (top 3% of reviewers). Moreover, he was named a Top Peer Reviewer (top 1% of reviewers) in Cross-Field and Computer Science in the Global Peer Review Awards 2019, which was presented by the Web of Science and Publons. Finally, in 2021, he received the best oral presentation award in the International Conference on Modern Circuits and Systems Technologies (MOCAST) 2021. He has been involved as a member of organizational and technical program committees in several IEEE and non-IEEE conferences and served as a reviewer in various IEEE journals and conferences. He is an IEEE Senior Member and a Member of the Technical Chamber of Greece. He is currently an editor for IEEE COMMUNICATIONS LETTERS, an associate editor for the Frontier in Communications and Networks, and for the MDPI Telecom.

Angeliki Alexiou is a professor at the Department of Digital Systems, ICT School, University of Piraeus. She received a diploma in electrical and computer engi-neering from the National Technical University of Athens in 1994 and a PhD in electrical engineering from Imperial College of Science, Technology and Medicine, University of London in 2000. Since May 2009 she has been a faculty member at the Department of Digital Systems, where she conducts research and teaches undergraduate and postgraduate courses in broadband communications and advanced wireless technologies. Prior to this appointment she was with Bell Laboratories, Wireless Research, Lucent Technologies, (later Alcatel-Lucent, now NoKIA), in Swin- don, UK, first as a member of technical staff (January 1999- February 2006) and later as a technical manager (March 2006-April 2009). Professor Alexiou is a co-recipient of Bell Labs President's Gold Award in 2002 for contributions to Bell Labs Layered Space-Time (BLAST) project and the Central Bell Labs Teamwork Award in 2004 for role model teamwork and technical achievements in the IST FITNESS project. Professor Alexiou is the Chair of the Working Group on Radio Communication Technologies and of the Working Group on High Frequencies Radio Technologies of the Wireless World Research Forum. She is a member of the IEEE and the Technical Chamber of Greece. Her current research interests include a radio interface for systems beyond 5G, MIMo, THz wireless technologies and reconfigurable intelligent surfaces, efficient resource management for ultra-dense wireless networks, machine-to-machine communications and artificial intelligence and machine learning for future wireless systems. She is the project coordinator of the H2020 TERRANoVA project (ict-terranova.eu) and the technical manager of H2020 ARIADNE project (ict-ariadne.eu).